COMMUNICATION

The intercalation of 1,10-phenanthroline into layered $NiPS_3$ via iron dopant seeding

Received 00th January 20xx,
Accepted 00th January 20xx

DOI: 10.1039/x0xx00000x

Xiaoping Ma[ab], Lu Zhang[ab], Chengchao Xu[ab], Qingxin Dong[ab], Richard I. Walton[c], Zian Li[ab], Honglong Shi[d], Genfu Chen[ab], Jiangping Hu[ab], Jianqi Li*[abe] and Huaxin Yang*[abf]

Using 2% percent of iron dopants as reaction active sites yields a series of single crystals of 1,10-phenanthroline intercalated $NiPS_3$, *via* solution reaction with aniline chloride, not possible by direct reaction. Experimental magnetic susceptibility measurements demonstrate that 1,10-phenanthroline intercalation suppresses the anti-ferromagnetism ordering at around 150 K in $Fe_{0.02}Ni_{0.98}PS_3$, and gives rise to a ferrimagnetic phase transition at the temperature around 75 K. An intercalation mechanism is proposed for the reaction, and this dopant seeding method provides a new approach for intercalation into layered materials.

The intercalation chemistry of ternary transition-metal phosphorus tri-chalcogenides MPX_3 (M=3d transition metal; X=chalcogenide) has attracted extensive attention due to their numerous properties for application in batteries, high performance catalysis and optoelectronics.[1-3] In recent years, interest has been paid to their electronic and magnetic properties. For example, MPX_3 shows diverse AF ordering states; $MnPS_3$ largely behaves like a Heisenberg antiferromagnet, while $FePS_3$ has the properties of an Ising antiferromagnet. Furthermore, superconductivity has been observed in $FePSe_3$ with the highest T_c of about 5.5 K achieved by suppressing AF order with external pressure, showing resemblance to high T_c cuprates and iron-based superconductors.[5] *Ab initio* study calculations also suggests that for single-layer APX_3, competition between anti-ferromagnetic and ferromagnetic states can be substantially influenced by gating and by strain engineering; the sensitive interdependence between magnetic, structural, and electronic properties suggests the potential of this 2D materials class for applications in spintronics.[5,6] Very recently, Hu *et. al.,* proposed that Ni-based transition-metal tri-chalcogenides are a promising platform to study exotic topological phenomena emerging from electronic correlation effects and that the emergence of topological superconductivity may be possible in Ni-based trichalcogenides.

Intercalation of organic species into layered inorganic solids provides a useful approach to creating ordered organic-inorganic nanocomposite materials with novel properties distinct from the parent compounds, which has attracted considerable attention. For example, the T_c of iron-based superconductor FeSe is only 8 K, but dramatically increases up to 44 K by the intercalation of alkaline and alkaline-earth metals; moreover, and lithium and pyridine-intercalated $Li_x(C_5H_5N)_yFe_{2-z}Se_2$ exhibits superconductivity with T_c=45 K.[6] For lamellar MPX_3 compounds, two types of intercalation reaction have been reported: lithium intercalation in $NiPS_3$ and $FePS_3$ involves electron donation from guest to host, which causes valence state change of the transition metal,[2,7,8] while for MPS_3 (M=Mn, Fe, Cd, Zn), some of the M cations may be removed during intercalation by strong complexation with a ligand and the charged vacancies are later balanced by protonated guest cations, therefore the valence state of the transition metal remains unchanged.[2-4,7,9] But so far there are no detailed intercalation investigations with $NiPS_3$ reported with organic species. In this communication, we report the intercalation of complexing agent 1,10-phenanthroline into layered $NiPS_3$ in solution with aniline chloride by using iron dopants as reaction active sites, and a series of single crystals of the solid solution $Fe_xNi_{1-x}PS_3$ and *N*, *N*-dimethylformamide (DMF) intercalated $Fe_xNi_{1-x}PS_3$ has also been synthesised (see S1).

Powder X-ray diffraction measurements were used to characterise the structure of $Fe_xNi_{1-x}PS_3$ samples and Fig. 1a shows the experimental data for samples with nominal compositions of x from 0 to 1. It was previous reported that the family all have monoclinic symmetry with space group *C*2/*m*; the lattice parameters are *a*=5.9681 Å, *b*=10.2925 Å, *c*=6.7229 Å and β =107.374° for $FePS_3$, and *a*=5.7978 Å, *b*=10.1074 Å, *c*=6.6265 Å and β =107.050°, for $NiPS_3$, which is consistent with the larger ionic radius of Fe^{2+} compared to Ni^{2+}. Profile refinement of the powder XRD for the $Fe_xNi_{1-x}PS_3$ samples shows that the lattice parameters increase progressively with

[a] Beijing National Laboratory for Condensed Matter Physics, Institute of Physics, Chinese Academy of Sciences, Beijing, 100190, China
[b] School of Physical Sciences, University of Chinese Academy of Science, Beijing, 100190, China.
[c] Department of Chemistry, University of Warwick, Coventry CV4 7AL, UK
[d] School of Science, Minzu University of China, 27 Zhong guancun South Avenue, Haidian District, Beijing, 100081, China
[e] Songshan Lake Materials Laboratory, Dongguan, Guangdong, 523808, China
[f] Yangtze River Delta Physics Research Center Co., Ltd., Liyang, Jiangsu, 213300, China

Electronic Supplementary Information (ESI) available: Experimental details (S1) and the lattice parameters of $Fe_xNi_{1-x}PS_3$ (Table S1) See DOI: 10.1039/x0xx00000x

the increase of the Fe content (Table S1), confirming the successful substitution of Ni by Fe in $Fe_xNi_{1-x}PS_3$. The inset of Fig. 1a shows the (001) Bragg peak, showing a shift to lower angle with increased Fe content. Fig. 1b presents a typical example of EDX spectrum from a piece of single crystal, which confirms the presence of the Ni, Fe, P and S, and the composition of the material is estimated as $Fe_{0.02}Ni_{0.98}PS_3$. The inset of Fig.1b shows a SEM image illustrating the morphological features of $Fe_{0.02}Ni_{0.98}PS_3$ crystal grains, where layered structural features can be easily observed. All the $Fe_xNi_{1-x}PS_3$ materials show similar morphological features and a chemical composition very close to the expected nominal composition. The crystal structure of $Fe_{0.02}Ni_{0.98}PS_3$ was tested by electron-diffraction patterns taken along the [001] zone axis Fig. 1c, in which all primary diffraction spots can be good agreement with the XRD data.

We find that no intercalation is observed for pure $NiPS_3$ using complexing agent 1,10-phenthroline with aniline chloride in DMF even with prolonged reaction time. Fig. 2a shows the XRD patterns of the $Fe_{0.02}Ni_{0.98}PS_3$ samples taken out at six different reaction times, which is typical for all $Fe_xNi_{1-x}PS_3$ precursors. At the early stage, only the patterns of pure $Fe_xNi_{1-x}PS_3$ were observed. After 1 day of reaction, there are two phases, pristine $Fe_xNi_{1-x}PS_3$ and a new phase, and as the period of intercalation is prolonged, the XRD reflections of pristine $Fe_xNi_{1-x}PS_3$ phase gradually disappear and the new phase predominates. Finally, the pure intercalation phase is obtained after 9 days. Detailed analysis suggests the intercalated $Fe_{0.02}Ni_{0.98}PS_3$ product, the lattice parameters are a=5.7821 Å, b=10.0902 Å, c=15.6254 Å and β =107.115°, the increase of lattice spacing is about Δc=8.9979 Å compared with the $Fe_{0.02}Ni_{0.98}PS_3$ precursor. Table S1 lists the lattice parameters obtained from our XRD experiments. It is clear that for the intercalates, a and c increase with the increase of Fe substitution level, x. The increase of the lattice parameters can be explained by the co-contribution of the increase of the lattice parameters of the $Fe_xNi_{1-x}PS_3$ starting materials and the slight increase of the inserted 1,10-phenanthroline guest species. Fig. 2b shows the EDX spectrum of the intercalated $Fe_{0.02}Ni_{0.98}PS_3$ product, where no Fe was detected, and Ni, P and S with a 0.98:1:3 atomic ratio, indicating that the 1,10-phenathroline intercalation process extracts all of the Fe. An SEM image of a typical intercalation product with evident layered structure shown in the inset of Fig. 2b, and a diffraction pattern taken from the [001] zone axis is shown in Fig. 2c, demonstrating that despite the significant increase of the interlayer space due the intercalation of 1,10-phenathroline, the intralayer structure is similar to the $Fe_xNi_{1-x}PS_3$ precursors.

A possible intercalation mechanism of intercalation reaction of 1,10-phenanthroline with layered $FePS_3$ in ethanol and in the presence of anilinium chloride was previously proposed by Chen *et al.*[9] who suggested the intercalation is a non-redox reaction, and as a result of intercalation, the increase of interlayer lattice spacing of 9.0 Å with respect to pure $FePS_3$ indicates that the 1,10-phenanthroline molecular ring is oriented perpendicular to the layer of the host when excess 1,10-phenanthroline is used in the reaction. A smaller increase of interlayer lattice spacing of 3.5 Å would show that the guest is parallel to the layer when a suitable amount of phenanthroline is used.[3]

From the results we propose a possible intercalation mechanism for 1,10-phenanthroline inserted into $Fe_xNi_{1-x}PS_3$ (see Steps. 1 to 3) in Fig. 3, in which 1,10-phenthroline acts as a complexing agent to remove intralamellar iron ion into solution during intercalation and leads to the presence of the Fe^{2+} vacancies in the Ni-P-S layers, and aniline chloride provides a proton to 1,10-phenthroline. The intercalation of $Fe_xNi_{1-x}PS_3$ is then achieved by charge attraction between the charged vacancy defective point and the protonated 1,10-phenanthroline, so that the charge neutrality of the intercalation is maintained.[3, 7,10-13] Our results also suggest that the intercalation is triggered by the doped Fe as active centre and that no Ni is involved in the whole process, consistent with the fact that no intercalation is observed on pure $NiPS_3$, no matter how long the time and how much 1,10-phenthroline and aniline chloride is used.

Fig. 4a shows the IR spectra of pure $Fe_{0.02}Ni_{0.98}PS_3$, intercalated $Ni_{0.98}PS_3$, neutral phenanthroline and anilinium chloride. In general, 1,10-phenanthroline intercalates have three sharp absorption peaks at around 614, 576, and 553 cm^{-1} in the range 550 to 650 cm^{-1}, indicating the presence of intralamellar transition metal. It has been

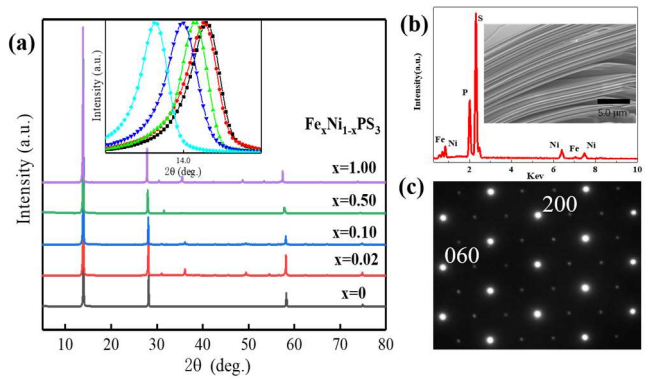

Fig. 1(a) XRD patterns of $Fe_xNi_{1-x}PS_3$, showing the increase of the interlayer distance with the increase of Fe content. (b) EDX spectrum and a SEM image of a piece of $Fe_{0.02}Ni_{0.98}PS_3$ single crystal. (c) Selected-area electron diffraction patterns of $Fe_{0.02}Ni_{0.98}PS_3$ taken along the [001] zone-axis direction.

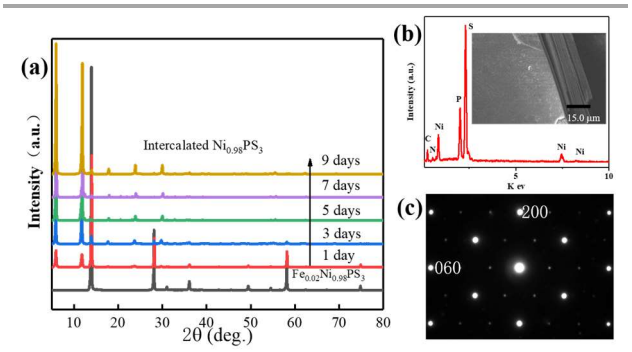

Fig. 2(a) XRD patterns used to monitor the intercalation of $Ni_{0.98}PS_3$ with 1,10-phenthroline. (b) The EDX spectrum and a typical SEM image of a final intercalated product. (c) Selected-area electron diffraction patterns taken along the [001] zone-axis direction of the final intercalated product $Ni_{0.98}PS_3$ product.

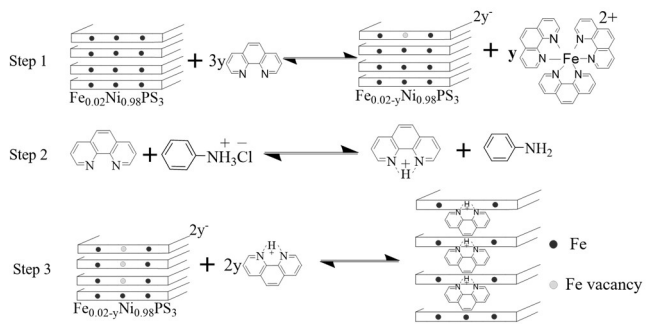

Fig.3 Intercalation mechanism of 1,10-phenanthroline with layered $Fe_{0.02}Ni_{0.98}PS_3$. Step 1: doped Fe^{2+} reacted as active centre removed initially by 1,10-phenanthroline. Step 2: proton transfer between 1,10-phenanthroline and aniline chloride. Step 3: the protonated 1,10-phenanthroline inserted into the layer to balance charge neutrality is perpendicular to the layer of the host.

previously shown that the occurrence of the intralamellar M^{2+} vacancies in MPS_3 makes the P–S bonds in the PS_3 groups unequivalent, which causes asymmetric $\nu(PS_3)$ stretching vibrations of the host and gives rise to the splitting of the 575 cm^{-1} peaks.[2,3,14] Fig. 4b shows the UV spectra of the filtrate of reaction mixture after intercalation, where an absorption peak around 510 nm is seen, which is characteristic for $Fe(phen)_3^{2+}$, indicating the 1,10-phenanthroline complexes the doped iron in $Fe_{0.02}Fe_{0.98}PS_3$, removing it into solution as $Fe(phen)_3^{2+}$ during the intercalation reaction.[2] The infrared spectra of the intercalated compounds show similar characteristic absorption bands (at around 1616, 1593, 1421, 1094, 843, and 723 cm^{-1}) to those of molecular phenanthroline, which proves the existence of phenanthroline based species as a guest.[2,3] In order to prove that the intercalated guest species is protonated phenanthroline, we added acetic acid instead of anilinium chloride as proton provider in the reaction mixture, which can also successfully trigger the intercalation reaction. However, without adding acid in the reaction mixture, no intercalation occurs for $Fe_{0.02}Ni_{0.98}PS_3$, even though the $Fe(phen)_3^{2+}$ can be detected in the filtrate. These experiment results support the conclusion that the protonation of phenanthroline is essential for intercalation and the guest intercalated into the layer is protonated phenanthroline. Further evidence is provided by IR spectroscopy (see Fig.2S).

Our model is further supported by the thermogravimetric (TG) analysis and differential thermal analysis (DTA) shown in Fig. 5a. The first mass loss can be assigned to the deintercalation of protonated 1,10-phenanthroline. The mass loss derived from the measurement is 3.80%, consistent with the mass of protonated 1,10-phenanthroline that compensates for the vacancies left by Fe^{2+}: if the doped Fe is fully reacted, there should be 3.77 % protonated 1,10-phenanthroline present. This confirms that the 1,10-phenathroline only extracts Fe and therefore that the protonated 1,10-phenathroline achieves intercalation into $Fe_xNi_{1-x}PS_3$ by charge attraction so that charge neutrality is maintained. When the doped Fe content, x, increases to x=0.1, 0.5 and 1, the mass loss of protonated 1,10-phenanthroline from TG measurement, is 7.55, 10.46 and 13.41%, respectively, which corresponds to 4.0%, 5.5%, and 7.1% intralamellar vacancy concentration in $Fe_xNi_{1-x}PS_3$, respectively. A further mass loss occurring from 600 to 700 °C corresponds to the decomposition of the compound.

The materials, $FePS_3$ and $NiPS_3$, show ordering anti-ferromagnetically at low temperatures, with the Néel temperature being 123 and 153 K, respectively.[4,15] The right hand inset of Fig. 5b shows the temperature dependent susceptibility for $Fe_{0.02}Ni_{0.98}PS_3$, which is similar to $NiPS_3$ with an antiferromagnetic phase transition at around 150 K. Fig. 5b shows the temperature dependent susceptibility curves of intercalation $Fe_{0.02}Ni_{0.98}PS_3$ with 1,10-phenthroline in different magnetic fields, and the Curie-Weiss fitting curve. Fig. 5c shows $\chi \times T$-T and $1/\chi$-T curve of magnetic field H=0.1 T. The magnetism of the intercalated sample is different to the precursor $Fe_{0.02}Ni_{0.98}PS_3$ that the anti-ferromagnetic phase at around 150 K no longer exists. As shown in Fig. 5c the $1/\chi$-T curve above 100 K is in good agreement with the Curie-Weiss law with a Weiss constant of $\theta = -396.56$ K. The negative Weiss constant indicates the existence of the antiferromagnetic interactions between the localized Ni^{2+} ions in the paramagnetic range. It can be seen clearly that the $\chi \times T$-T curve at 75 K exhibits a sudden upward turn, suggesting the existence of a ferrimagnetic phase transition.[3,15,16] Fig. 5d shows hysteresis loop measurements at temperatures, T=80, 40 and 1.80 K. The magnetic hysteresis

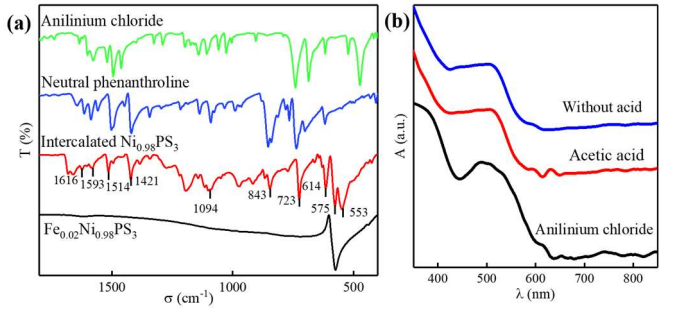

Fig. 4(a) IR spectra of pure $Fe_{0.02}Ni_{0.98}PS_3$, 1,10-phenanthroline intercalated $Ni_{0.98}PS_3$, neutral phenanthroline and anilinium chloride. (b) The UV spectra of the filtrates of reaction mixture after intercalation reaction.

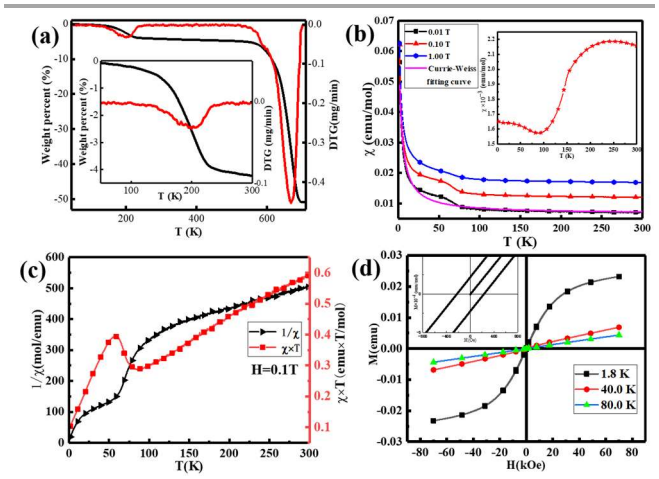

Fig. 5(a) The TG and DTG curves for the final intercalated $Ni_{0.98}PS_3$ product from 30 to 700 ℃, and the inset is the zoomed figure in the range of 40-300℃. (b) Temperature dependence of the magnetic susceptibility of intercalated $Ni_{0.98}PS_3$, the right hand inset shows the χ-T curve of pristine $Fe_{0.02}Ni_{0.98}PS_3$. (c) The 1/χ-T and χ×T-T curves of intercalated $Ni_{0.98}PS_3$ in H=0.1 T. (d) The hysteresis loop measurements at temperature, T=1.8, 40 and 80 K, respectively, and the inset shows the hysteresis loop zoomed figure in range of from -800 to 800 Oe at temperature, T=1.8 K.

loop with coercivity (320 Oe) found at 1.8 K further suggests that the intercalation compound is a low-temperature ferrimagnet. In $NiPS_3$, the magnetic order is a zig-zag stripe type of anti-ferromagnetism (AFM). The main AFM interactions stem from the two-third nearest neighbour Ni atoms while the first- and second-nearest neighbour magnetic interactions are ferromagnetic.[16] In the 1,10-phenanthrolne intercalated $Fe_xNi_{1-x}PS_3$ samples, the local lattice distortion caused by the vacancy - significantly increases those ferromagnetic interactions locally to cause the observed ferromagnetic signal because they are very sensitive to the change of the local angles of Ni-S-Ni.

Further experiments show that Co and Mn doped $NiPS_3$ have a very similar 'seeding' effect.. XRD patterns of $Co_{0.02}Ni_{0.98}PS_3$ and $Mn_{0.02}Ni_{0.98}PS_3$ and their corresponding 1,10 phenanthroline intercalations are shown in Fig. 6S. In summary, a series of $Fe_xNi_{1-x}PS_3$ ($0 \leq x \leq 1$) single crystals and their corresponding 1,10-phenanthroline intercalated compounds have been synthesised. As a result of intercalation, the lattice parameter of the *c* axis is expanded by 8.9979 Å with respect to pure $Fe_{0.02}Ni_{0.98}PS_3$. It is found that the 1,10-phenathroline only extracts Fe and the protonated 1,10-phenathroline achieves intercalation into $Fe_xNi_{1-x}PS_3$ by charge attraction so that the charge neutrality of the intercalation is maintained. $Fe_xNi_{1-x}PS_3$ materials show anti-ferromagnetic ordering at low temperature, and the anti-ferromagnetic ordering in pure $Fe_xNi_{1-x}PS_3$ was suppressed after intercalation and instead gives rise to a ferrimagnetic phase transition at the temperature of about 75 K. The dopant seeding method could be applicable to other intercalation reaction to allow access to phases not accessible by other methods.

This work was supported by the National Key Research and Development Program of China under Grant Nos. 2016YFA0300303, 2017YFA0504703, 2017YFA0302904, and 2017YFA0303000, the National Basic Research Program of China under Grant No. 2015CB921304, the National Natural Science Foundation of China under Grant Nos. 11774391, 11774403 and 11804381, the Strategic Priority Research Program (B) of the Chinese Academy of Sciences under Grant No. XDB25000000, XDB07020000, the Scientific Instrument Developing Project of the Chinese Academy of Sciences under Grant No. ZDKYYQ20170002.

Conflicts of interest

There are no conflicts to declare.

Notes and references

1 (a) Q. Pei, Y. Song, X.C. Wang, J.J. Zou and W.B. Mi, Sci. Rep., 2017, 7, 9504; (b) Q. Pei, Y. Song, X. C. Wang, J. J. Zou and W. B. Mi, Nanotechnology, 2018, 29, 214001; (c) C. F. Du, Q. H. Liang, R. Dangol, J. Zhao, H. Ren, S. Madhavi and Q. Y. Yan, Nano-Micro Lett., 2018, 10, 67; (d) C. Tang, H. S. Wang, H. F. Wang, Q. Zhang, G. L. Tian, J. Q. Nie and F Wei, Adv. Mater., 2015, 27, 4516; (e) B. Konkena, J. Masa, A. J. R. Botz, I. Sinev, W. Xia, J. Koßman, R. Drautz, M. Muhler and W.Schuhmann, ACS Catal., 2017, 7, 229; (f) M. A. Susner, M. Chyasnavichyus, M. A. McGuire, P. Ganesh and P. Maksymovych, Adv. Mater., 2017, 29, 1602852; (g) C. C. Mayorga-Martinez, Z. Sofer, D. Sedmidubský, Š. Huber,A. Y. S. Eng and M. Pumera, ACS Appl. Mater., 2017, 9,12563.

2 C. L. Yang, X. G. Chen, J. G. Qin, K. Y. Yakushi, Y. A. Nakazawa and K. J. Ichimura, J. Solid State Chemistry, 2000, 150, 281.

3 (a)X. B. Yan, X. G. Chen and J. G. Qin, Mater. Res. Bull., 2011, 46, 235;(b) X. G. chen, C. L. yang and J. G. qin, J. Solid State Chemistry, 2000, 150, 258.

4 (a) P. A. Joy and S. Vasudevan, Phys. Rev. B., 1992, 46, 5425; (b) B. L. Chittari, Y. Park, D. Lee, M. Han, A. H. Macdonald, E. Hwang, and J. Jung, Phys. Rev. B., 2016, 94, 184428; (c)Y. G. Wang, J. J. Ying, Z. Y. Zhou, J. L. Sun, V. V. Struzhkin, Y. S. Zhao and H. K.Mao, Nat. Commun., 2018, 9, 1914.

5 (a) N. Sivadas, M. W. Daniels, R. H. Swendsen, S. Okamoto, and D. Xiao, Phys. Rev. B., 2015, 91, 235425; (b) A. R. Wildes, V. Simonet, E. Ressouche, G. J. McIntyre, M. Avdeev, E. Suard, S. A. J. Kimber, D. Lancon, G. Pepe, B. Moubaraki, and T. J. Hicks, Phys. Rev. B, 2015, 92, 224408.

6 (a) Y. X. Li, X. X. Wu, Y. H. Gu, C. C. Le, S. S. Qin, R. Thomale and J. P. Hu, arXiv, 1906, 05999; (b)Y. H. Gu, Q. Zhang, C. C. Le, Y. X. Li, T. Xiang and J.P. Hu, Phys. Rev. B., 2019, 100, 165405; (c) A. Krzton-Maziopa, E. Pesko, and R. Puzniak, J. Phys.Condens. Matter, 2018, 30, 243001.

7 (a) C. T. Kuo, M. Neumann, K. Balamurugan, H. J. Park, S. Kang, H. W. Shiu, J. H. Kang, B. H. Hong, M. Han, T.W. Noh and J. G. Park, Sci. Rep., 2016, 6, 20904;

8 (a) X. Zhang, H. Q. Zhou, X. Su, X. G. Chen, C. L. Yang, J. G. Qin, M. Inokuchi, J. Alloys Comp., 2007, 432, 247; (b) X. Zhang, X. G. Chen, X. Su, C. L. Yang, J. G. Qin and M. K. Inokuchi, J. Solid State Chemistry, 2004, 177, 2014.

9 G. Giunta, V. Grasso, F. Neri, and L. Silipigni, Phys. Rev.B., 1994, 50, 8189.

10 (a) A. Leaustic, E. Riviere and R. Clement, Chem. Mater., 2003, 15, 4784; (b) J. S. O. Evans, S. Benard, P. Yu and R. Clement, Chem. Mater., 2001, 13, 3813; (c) X. G. Chen, Z. Li, H.Q. Zhou, T. J. Wang, J. G. Qin and M. Inokuchi, Polymer,2007, 48, 3256; (d)R. Clement, L. Lomas, and J. P. Audiere, Chem. Mater. 1990 2, 641.

11 A. Leaustic, J. P. Audiere, P. G. Lacroix, R. Clement, L. Lomas, A. Michalowicz, W. R. Dunham, and A. H. Francis, Chem. Mater. 1995, 7, 1103.

12 (a) J. Qin, C. Yang, K. Yakushi, Y. Nakazawa, and K. Ichimura, Solid State Commun. 1996, 100, 427; (b) H. Q. Zhou, X. Su, X. Zhang, X. G. Chen, C. L. Yang, J. G. Qin and M. Inokuchi, Mater. Res. Bull., 2006, 41, 2161.

13 H. Loboue, C. G. Deudon, A. F. Popa, A. Lafond, B.Rebours, C. Pichon, T. Cseri, G. Berhault and C.Geantet, Catal.Today., 2008, 130, 63.

14 (a) X. Chen, H. Zhou, L. Zou, C. Yang, J. Qin, M. Inokuchi, J. Incl. Phenom. Macrocycl. Chem. 2005, 53, 205; (b) A. Leaustic, J. P. Audiere, D. Cointereau, R. Clement, L. Lomas, F. Varret, H. Constant-Machado, Chem. Mater. 1996, 8, 1954.

15 (a) J. U. Lee, S. Lee, J. H. Ryoo, S. Kang, T. Y. Kim, P.Kim, C. H.Park, J. G. Park and H. Cheong, Nano Lett., 2016, 16, 7433; (b) A. R. Wildes, V. Simonet, E. Ressouche, G. J. McIntyre, M. Avdeev, E. Suard, S. A. J. Kimber. Lanc ¸on, G. Pepe, B. Moubaraki, and T. J. Hicks, Phys. Rev. B., 2015, 92, 224408;

16 V. Manrı´queza, P. Barahonaa and O. Pen, Mater. Res. Bull., 2000, 35, 1889.

